sciendo

POLISH MARITIME RESEARCH 3 (119) 2023 Vol. 30; pp. 153-162
10.2478/pomr-2023-0048

EXPERIMENTAL STUDY OF THE NONLINEAR BEHAVIOUR OF DEEP-SEA MOORING POLYESTER FIBRE ROPES

He Zhang [1]
Ji Zeng * [2]
Bowen Jin [1]
Chiate Chou [3]
Hangyu Li [3]
Hailei Dong [3]
[1] Merchant Marine College, Shanghai Maritime University, Shanghai, China
[2] College of Ocean Science and Engineering, Shanghai Maritime University, Shanghai, China
[3] Zhejiang Four Brothers Rope Co. Ltd., Taizhou, China

* Corresponding author: *zengji@shmtu.edu.cn (Ji Zeng)*

ABSTRACT

Mooring ropes are essential components of ships and offshore floating structures and they are subjected to cyclic axial loads. This study investigates the evolution of the full-cycle stiffness of fibre polyester ropes under long-term static and dynamic loading. First, the static stiffness characteristics of the ropes, including the rope elongation properties at different stages, shrinkage rates, and creep coefficients after an idle period, are examined under static loads; an empirical formula for static stiffness is established. Second, the dynamic stiffness characteristics of the ropes are investigated under cyclic loads that are typical of platform production operations. The stabilities of the structure under different tensions are compared; the effects of mean tension, tension amplitude, and load cycle on the dynamic stiffness of the ropes are analysed and an empirical formula is established to predict the dynamic stiffness during the engineering design phase. The results of this study can be helpful for the rational design of deep-sea taut-leg mooring systems because they present the evolution of the full-cycle stiffness characteristics of mooring ropes.

Keywords: polyester fibre ropes; static stiffness; creep coefficient; long-term cyclic loads; dynamic stiffness

INTRODUCTION

As China continues to implement its marine strategy, the development of deep-sea oil and gas resources has become important for strengthening its maritime power. This development depends on the support of platform-positioning technology, and mooring ropes play a decisive role in the lifeline of the mooring system. In the 1960s, Vecchio and Moraes [1] proposed using synthetic fibres in deep-water taut-leg mooring systems. Kota et al. [2] compared the mooring performances of polyester ropes and steel cables at water depths of 1000–3000 m and found that polyester ropes were more advantageous compared with steel cables. However, unlike steel cables, synthetic fibre materials exhibit viscoelastic and viscoplastic behaviour [3], and the stretching behaviour of ropes made of such materials exhibits nonlinear characteristics, which are influenced by factors such as load size and frequency. To understand the mooring performances of floating structures, numerous researchers have conducted extensive investigations on the mechanical properties of synthetic fibre ropes.

To examine the tensile properties of ropes, the American Bureau of Shipping (ABS) [4] developed a method for detecting their breaking strengths, which is one of the simplest mechanical parameters. Beltran and Williamson [5–7] established a numerical analysis model to study changes in the static curve and breaking strength under monotonic loading. This model can be used to predict rope performance under various loads. Williams et al. [8], Lanquetin et al. [9], and Lian et al. [10] evaluated the effects of different degrees of damage on the tensile forces of ropes by considering specimens with structural damage states. This

can further help us to understand the changes in mechanical performance when ropes are damaged during use. Davies et al. [11] found that most researchers only focused on the impact of the form of the load on the tension of ropes and ignored the impact of synthetic materials and weaving techniques. Therefore, they considered the influences of these factors on rope performance. Li et al. [12] considered the weaving structure and rope diameter in their mechanical research and further explored the influence of the rope's structure on its mechanical characteristics. Bain et al. [13] studied specific quantitative indicators of rope wear and the effects of different loading directions and strengths on stretching behaviour. These studies provide an important theoretical basis and experimental references for the design, manufacturing, and use of ropes.

Stiffness is one of the indicators used to determine the flexibility and bending performance of ropes and it is an important parameter for evaluating their performance and safety in engineering applications. In practical engineering, an appropriate assessment of rope stiffness can help engineers and designers choose suitable rope materials and structural forms, thereby ensuring the safety, reliability, and service life of ropes. Suitable testing methods and analytical tools are needed to accurately measure and analyse rope stiffness. Davies et al. [14] studied the dynamic stiffness evolution of three synthetic-fibre-rope types under short-term cyclic testing, namely: polyester, aramid, and high-molecular-weight polyethylene (HMPE). The results revealed that the mean tension was the main factor affecting the dynamic stiffness. Thus, they proposed an empirical formula for dynamic stiffness by considering the influence of the mean tension. Subsequently, Liu et al. [15] conducted dynamic stiffness tests on aramid, polyester, and HMPE ropes, Lian et al. [16] conducted tests on polyester and HMPE ropes, and Davies et al. [11] conducted tests on HMPE and aramid ropes. The results showed that, in addition to the mean tension, the tension amplitude and load cycle have a considerable impact on dynamic stiffness. Therefore, an empirical formula that integrates these three factors was proposed to improve the accuracy of the prediction model. Xu et al. [17] applied the Kalman filter to identify the parameters of an empirical formula and found that the Kalman filter could estimate the parameters of the empirical expression reliably and accurately. These studies revealed that rope stiffness testing is important, not only for the installation and use of ropes in practical engineering applications, but also, for clarifying the mechanical behaviour of synthetic fibre ropes [18–20]. However, certain problems require further investigation owing to the different degrees of rope wear, uncertainty in the accurate determination of elongation and stiffness, and ambiguity in rope creep during stiffness testing.

In this study, the axial tensile and complete stiffness characteristics of polyester ropes under load conditions were investigated through tension tests. To ensure the uniformity of the internal force on the rope, an empirical formula for stiffness was established by combining experimental data, including the static stiffness of the rope after installation and aging, and the dynamic stiffness of the rope under the influence of different mean tensions, tension amplitudes, and load cycles, considering the creep coefficient.

BASES FOR POLYESTER FIBRE ROPE TESTS

STIFFNESS TEST EQUIPMENT

For the stiffness test, a 3000-t microcomputer-controlled horizontal heavy-duty tension-testing machine (Zhejiang Four Brothers Rope Co., Ltd.) was used. The machine consists of an equipment base, a stator-end/stator hydraulic device, a test-end/test hydraulic device, and a water environment system, as shown in Fig. 1 [21]. The tensioner was 22 m long, with a capacity of 3000 t and a maximum error of 0.2%. The tests were conducted at room temperature (25°C) and 65% humidity. The elongation rate ΔL of the test rope was recorded four times per second using displacement sensors and strain gauges.

Fig. 1. Structural diagrams of 3000-t and rope-tension-reciprocating testing machine

For the test specimen, a polyester fibre rope with 1 × 12 strands was selected. Its parameters are specified in Table 1. The rope specimen was fixed to the testing equipment using the eye-splice method. The total length of the rope specimen was 14 m, which included an eye-splice length of approximately 3 m. To avoid the influence of eye-splice weaving on the mechanical properties of the rope and ensure that the rope specimen had a sufficient undisturbed area, the middle L_0 = 5 m segment was selected for measurements during the test, as shown in Fig. 2.

Tab. 1. Specifications of the polyester fibre rope test specimen

	Material	Pitch	Weaving	Diameter	Total length	Minimum breaking strength
Specimen	Polyester	300 mm	1 × 12 strands	68 mm	14 m	1786.4 kN

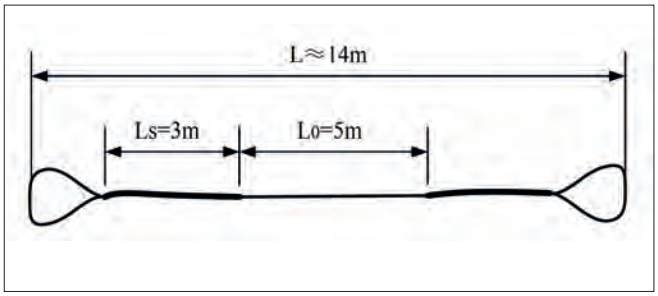

Fig. 2 . Diagram of test segment of polyester fibre rope

STIFFNESS CALCULATION

The elongation characteristics of a rope are typically related to the morphological structure of the corresponding material. The internal structures of the fibres include crystalline and amorphous forms. When the force is slowly loaded, the crystalline and amorphous parts of the structure have sufficient reaction time to act on the external forces. The mean stiffness of these two parts is called the 'static stiffness' of the rope. When the rope is subjected to periodic loading, the amorphous part of the structure cannot respond quickly to external forces, and only the crystalline part bears the load. The stiffness of this part is defined as the 'dynamic stiffness'. Generally speaking, the dynamic stiffness of a rope is approximately 2–3 times greater than its static stiffness.

Rope stiffness can be calculated by Eq. (1), and Eq. (2), after normalisation using the minimum breaking strength (*MBS*).

$$EA = \Delta T / \Delta\varepsilon \tag{1}$$

$$K_r = EA / \mathrm{MBS} = \frac{(T_n^p - T_{n-1}^v) / MBS}{\varepsilon_n^p - \varepsilon_{n-1}^v} \tag{2}$$

where: E is the elastic modulus; A is the cross-sectional area; ΔT is the axial force increment; $\Delta\varepsilon$ is the strain increment; K_r is the stiffness coefficient; T_n^p and ε_n^p are the peak tension and corresponding strain in the n -th cycle, respectively; and T_{n-1}^v and ε_{n-1}^v are the valley tension and corresponding strain in the (n − 1)th cycle, respectively.

Here, K_r consists of a static stiffness coefficient, K_{rs}, and dynamic stiffness coefficient, K_{rd}. François and Davies [22] introduced the concept of 'quasi-static stiffness', to account for the influence of time-dependent characteristics of fibre mooring lines in mooring analysis. Additionally, the ABS has also defined the calculation method for static stiffness, as shown in Eq. (3).

$$K_{rs} = (T_2 - T_1) / [\varepsilon_2 - \varepsilon_1 + C\lg(t)], \tag{3}$$

where: T_1 is the initial tension; T_2 is the final tension; ε_1 is the initial strain; ε_2 is the final strain; C is the creep factor (its determination is reported in the next section); and t is the creep time.

The calculation of the dynamic stiffness coefficient consists of three types: an upper and lower boundary model, a single-factor model, and a multifactor model. In a previous study [23], experimental data regarding the dynamic stiffness of polyester mooring ropes were collected from the relevant literature and the factor T_m was found to be an important factor influencing the dynamic stiffness of the rope, thus leading to the derivation of Eq. (4) for its calculation. However, the precise definition of the values for the upper and lower boundaries in the model was not provided. In another study [14], the dynamic stiffness calculation in Eq. (5) was derived for polyester mooring ropes influenced by factor T_m, avoiding the drawback of uncertain boundary values.

$$\begin{cases} 1.\ K_{rd} = 23 + 0.25T_m & \textit{lower limit} \\ 2.\ K_{rd} = 17 + 0.2T_m & \textit{upper limit} \end{cases} \tag{4}$$

$$K_{rd} = 18.5 + 0.33T_m\,. \tag{5}$$

However, a series of model tests, conducted previously [24], revealed that the influence of the tension amplitude T_A and load cycle N on the dynamic stiffness cannot be ignored; a multifactor dynamic stiffness prediction formula was proposed, as shown in Eq. (6). In this study, a multifactor formula was adopted that considers the mean tension, tension amplitude, and load cycle to predict the dynamic stiffness of polyester ropes.

$$K_{rd} = \alpha + \beta T_m + \gamma T_A + \delta\lg(N)\,, \tag{6}$$

where: T_m is the ratio of the mean tension to the average breaking strength (%*MBS*); T_A is the ratio of the tension amplitude to the average breaking strength (%MBS); N is the number of cycles; and α, β, γ and δ are the parameters of the empirical formula.

To ensure the accuracy of the derived dynamic stiffness equation, the accuracy of the dynamic stiffness model is evaluated using the error ratio ΔK_{rd}, mean error (*ME*), and mean squared error (*MSE*), as shown in Eqs. (7)–(9).

$$\Delta K_{rd} = (K_{rd\circ} - K_{rd\circ\, m}) / K_{rd\circ\, m}\,, \tag{7}$$

$$ME = \frac{1}{n}\sum_{t=1}^{n}(K_{rd,m}^t - \bar{K}_{rd}^t)\,, \tag{8}$$

$$MSE = \frac{1}{n}\sum_{t=1}^{n}(K_{rd,m}^t - \bar{K}_{rd}^t)^2\,, \tag{9}$$

where: n is the sample size; $K_{rd,m}$ represents the experimental values of the dynamic stiffness of the model; $\bar{K}_{rd}$ represents the estimated values of the dynamic stiffness calculated using the nonlinear fitting function 'nlinfit' in MATLAB; and t is the number of steps in the discrete observation process.

STIFFNESS PRELOADING TEST

Before the stiffness tests were conducted, each sample rope was pre-processed by performing a preloading test. This test was conducted to determine whether the internal structure of the rope was stable and to ensure that each fibre in the rope was in an equivalent tensile state, thereby guaranteeing the accuracy of the subsequent tests. To simulate the marine environment better, the sample rope was immersed in freshwater for at least 4 h. A pre-processed sample rope was then installed between the two anchors of the tension-testing machine and a strain gauge and measuring gauge were attached to the test specimen to record the elongation of the rope. First, 1% MBS was applied and held for 5 min. Next, the load was gradually increased to 13% MBS and held for 2 h. Subsequently, the load was increased to 40% MBS and held for 3 h (if the load dropped by more than 5% MBS, it was increased back to 40% MBS). Finally, the load was reduced back to 13% MBS and held for 6 h to complete the installation of the preloading test.

Fig. 3 shows the variation in the test rope with the load during the preloading test. The maximum elongation rate of the sample rope was 6.49%, which decreased to 4.58% as the load decreased, thus indicating a positive correlation between the rope elongation rate and load size. After 6 h of static settling,

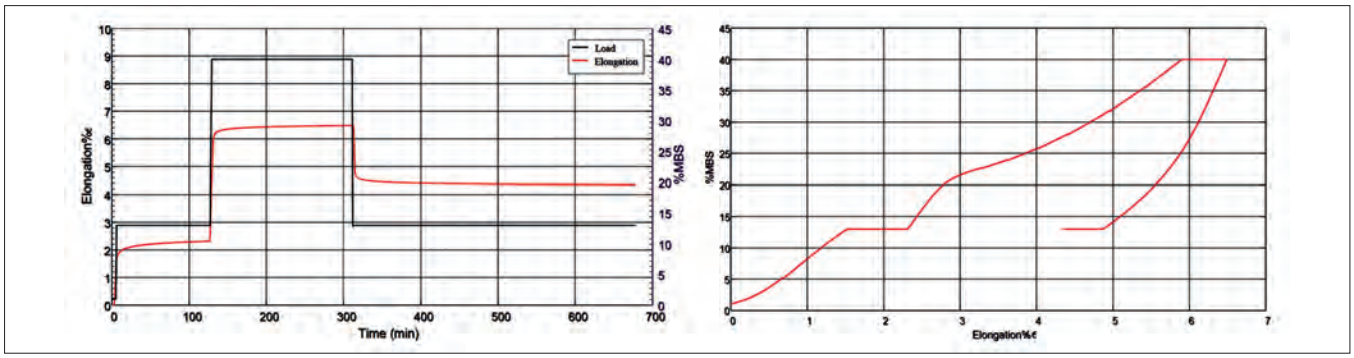

Fig. 3. Deformation of rope under different loads in the preloading test: (a) time-variation curve and (b) stress–strain curve

the elongation rate decreased to 4.345%, which is 0.23% less than that at the beginning of unloading. This indicates that some structural deformation inside the rope was not completely eliminated, thus resulting in a slight contraction of the rope. Therefore, fully tearing and wearing the rope is necessary.

STATIC STIFFNESS TEST OF POLYESTER FIBRE ROPES

The static stiffness test of the pre-treated ropes included initially installed ropes and aged ropes. In this study, periodic dynamic loads were considered to simulate the aging of the ropes. The pretension of 13% MBS was increased to 65% MBS and maintained for 100 min. Then, 1000 consecutive dynamic loads were applied within a tension range of 35–65% and cycles of 12–35 s. Finally, the tension of the last cycle was reduced to 13% MBS, and the aging of the rope was completed after 100 min. The experimental processes for studying the dynamic stiffness of the initially installed ropes and aged ropes were identical, and the specific force loading conditions are shown in Fig. 4.

The tensile characteristics, creep coefficients, and empirical formulas were determined for the static stiffness of the ropes at the installation stage under different loads. Fig. 4 shows that the tension during the static stiffness test process increased from 3% to 30% MBS and was maintained for 100 min. The tension was increased from 45% to 60% MBS and maintained for 100 min before unloading to the initial tension of 13% MBS. The strains of the ropes are shown in Fig. 5. The strains after loading and unloading of the initially installed and aged ropes were 7.835% and 7.952%, respectively; the corresponding strains for the pretension of 13% MBS were 5.192% and 5.441%. After remaining static for 200 min, the strains were 4.729% and 5.002%, respectively. The change in rope elongation shows that, after a static period, the initially installed and aged ropes shrank by 0.463% and 0.439%, respectively, and the shrinkage rates of the two were almost the same.

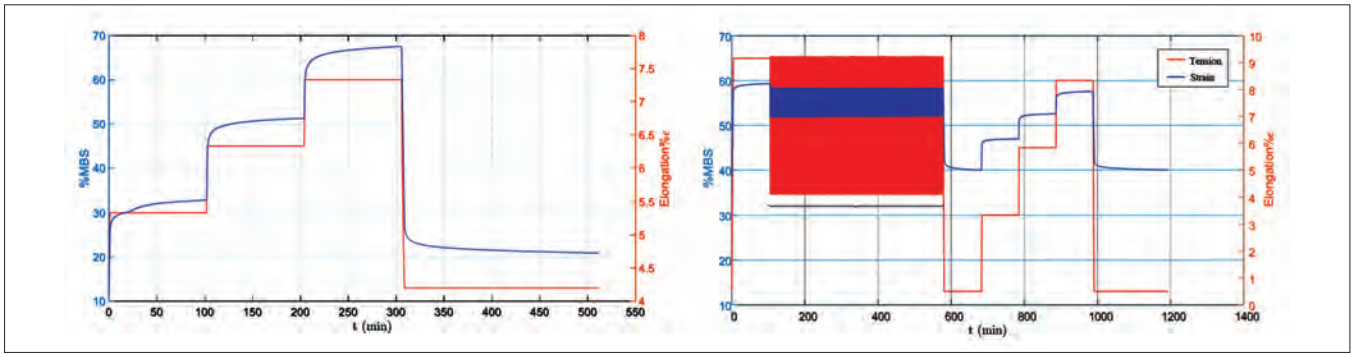

Fig. 4. Time curves of tension/strain in static stiffness test: (a) initially installed ropes and (b) aged ropes

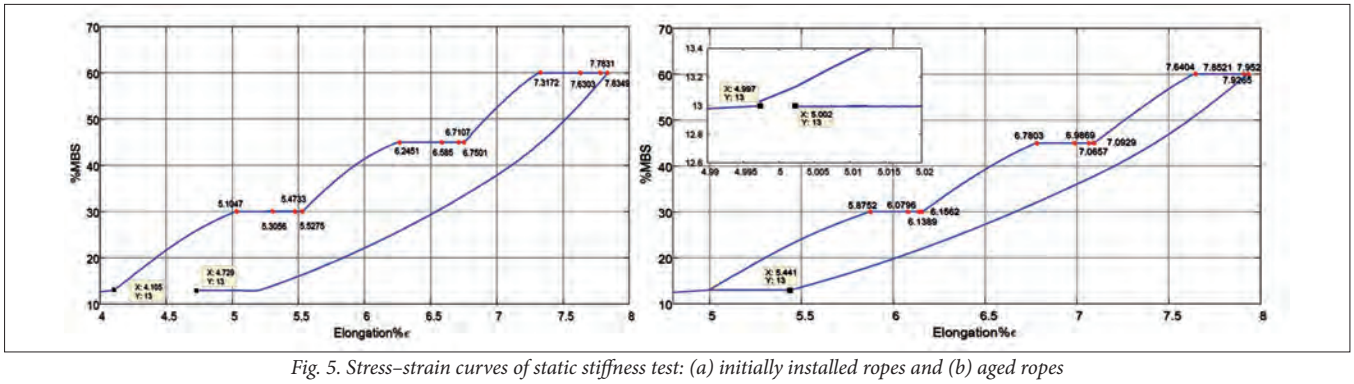

Fig. 5. Stress–strain curves of static stiffness test: (a) initially installed ropes and (b) aged ropes

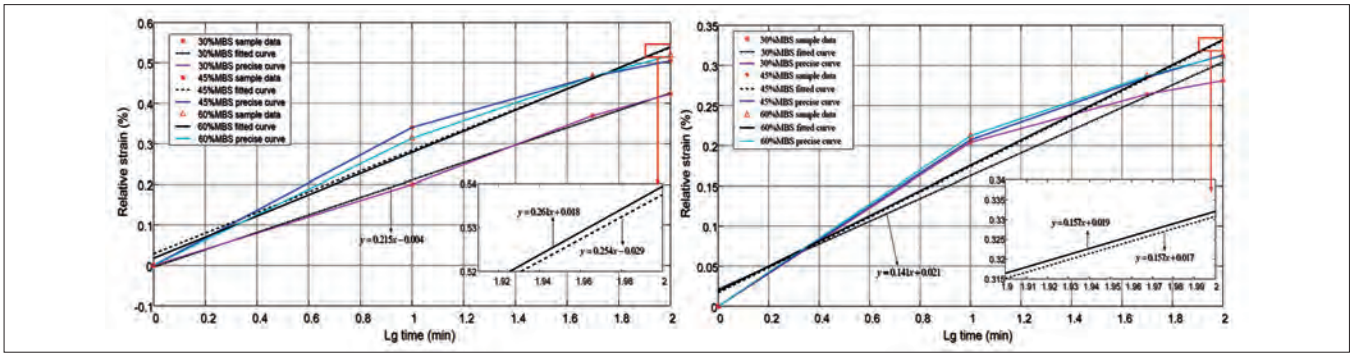

Fig. 6. Determination of creep coefficient of ropes based on static stiffness: (a) initially installed ropes and (b) aged ropes

Because different tensile loads correspond to unique creep coefficients, the rope elongation was measured and recorded at 1, 10, 50, and 100 min, to obtain the creep coefficients under different loads. For the convenience of calculation, the corresponding strain was assumed to be zero at the beginning of the test. The data for determining the creep coefficient under the static stiffness of the rope are presented in Table 2 and are derived from Fig. 5.

Tab. 2. Creep data for static stiffness testing of ropes with 30%, 45%, and 60% MBS

Load (%MBS)	Time (t, min)	Lg (t)	Initially installed rope strain (ε)	Aged rope strain (ε)	Relative strain of initially installed rope (%)	Relative strain of aged ropes (%)
30	1	0	5.1047	5.8752	0.000	0.000
30	10	1	5.3056	6.0796	0.200	0.204
30	50	Lg (50)	5.4733	6.1389	0.369	0.264
30	100	2	5.5275	6.1562	0.423	0.281
45	1	0	6.2451	6.7803	0.000	0.000
45	10	1	6.5850	6.9869	0.340	0.207
45	50	Lg (50)	6.7107	7.0657	0.466	0.285
45	100	2	6.7501	7.0929	0.505	0.313
60	1	0	7.3172	7.6404	0.000	0.000
60	10	1	7.6303	7.8521	0.313	0.212
60	50	Lg (50	7.7831	7.9265	0.466	0.287
60	100	2	7.8949	7.9520	0.518	0.312

The objective of this study was to determine the creep coefficient C, under different loads. The experimental data listed in Table 2 and the linear regression analysis performed using MATLAB software were utilised to obtain the results displayed in Fig. 6. As the applied load increased, the slopes of the regression curves for the initially installed and aged ropes increased in the order of 0.125, 0.254, and 0.261; and 0.141, 0.157, and 0.157, respectively. The creep rates corresponding to 30%, 45%, and 60% MBS were determined. As the tension load increased over time, the corresponding strain gradually increased, and the creep coefficient increased proportionally with the tension load. This indicates that the larger the tension load, the larger the creep coefficient of the rope.

The tension, strain, and fitted C values were substituted into Eq. (3) to solve the static stiffness equations for the ropes under 30%, 45%, and 60% MBS loads, as shown in Eq. (10). The derived formulas were used to predict the static stiffness of the rope material in advance and provide theoretical guidance for engineering production.

The dynamic stiffness values of initially installed ropes are:

$$\begin{aligned} K_{rs} &= 17/[1.423+0.144\lg(t)] \quad (\text{Load}=30\%\text{MBS}) \\ K_{rs} &= 32/[2.222+0.641\lg(t)] \quad (\text{Load}=45\%\text{MBS}) \\ K_{rs} &= 47/[2.802+0.171\lg(t)] \quad (\text{Load}=60\%\text{MBS}) \end{aligned} \tag{10}$$

The dynamic stiffness values of aged ropes are:

$$\begin{aligned} K_{rs} &= 17/[1.159+0.141\lg(t)] \quad (\text{Load}=30\%\text{MBS}) \\ K_{rs} &= 32/[1.815+0.157\lg(t)] \quad (\text{Load}=45\%\text{MBS}) \\ K_{rs} &= 47/[2.361+0.157\lg(t)] \quad (\text{Load}=60\%\text{MBS}) \end{aligned} \tag{11}$$

Fig. 7 shows a line graph of the six static stiffness equations derived, which can facilitate the prediction of static stiffness during the rope production and design phases. The load applied during the test can be considered to be equivalent to the actual forces the rope would experience in a marine environment. Fig. 7 shows that the static stiffness increases with increasing load and decreases with increasing duration of the load. Aged ropes exhibit greater static stiffness than initially installed ropes under the same load, primarily because aged ropes undergo sufficient wear and tear, thus resulting in less residual strain in the internal structure and a greater ability to resist external deformation.

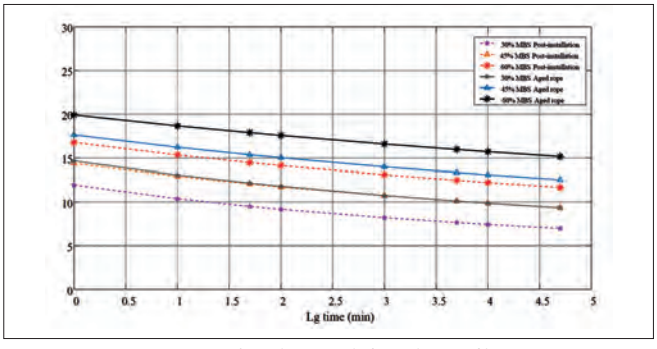

Fig. 7. Static stiffness line graph for polyester fibre ropes

DYNAMIC STIFFNESS TESTING OF POLYESTER FIBRE ROPES

The design of the dynamic stiffness test conditions for the polyester fibre ropes includes two main types of load: tension and tightening. The load cycles were selected based on the inherent periods of swaying, rolling, and heaving during the production operation of offshore floating platforms. The test conditions are listed in Table 3.

Tab. 3. Design of dynamic stiffness test conditions for polyester ropes

Test	Mean tension T_m (%MBS)	Tension amplitude T_A (%MBS)	Minimum tension T_{min} (%MBS)	Maximum tension T_{max} (%MBS)	Load cycle T_m (S)
1	15	2	13	17	30
2	15	5	10	20	30
3	15	2	13	17	150
4	15	3	12	18	150
5	35	10	25	45	40
6	35	15	20	50	15
7	35	15	20	50	150
8	40	10	30	50	40
9	40	20	20	60	40
10	40	15	25	55	15
11	40	15	25	55	150
12	50	10	40	60	40
13	50	15	35	65	15
14	50	15	35	65	150
15	60	10	50	70	15
16	60	10	50	70	150
17	60	15	45	75	30
18	65	5	60	70	150

The testing procedure for dynamic stiffness followed the following steps.

(1) For each wave frequency test case, the rope was cycled 40 times between T_{min} and T_{max}, and the load and elongation were recorded at a frequency of at least 1 Hz.

(2) For each low-frequency test case, the rope was cycled 20 times under tension between T_{min} and T_{max}, and the load and elongation were recorded at a frequency of at least 0.25 Hz.

(3) The test for the entire matrix was continuous without significant interruptions.

Fig. 8 shows the time-varying load in the dynamic stiffness testing of the rope. The parallel peaks and valleys of the tension in the figure indicate that the test system can provide long-term stable cyclic loads. Moreover, the graph indicates that this study considered the effects of three factors (mean tension, tension amplitude, and cycle period) on the dynamic stiffness of the rope. For example, tests 8–10 considered the effect of the tension amplitude on the dynamic stiffness, whereas the mean tension was the same. Tests 6, 10, and 13 considered the effect of the mean tension on the dynamic stiffness.

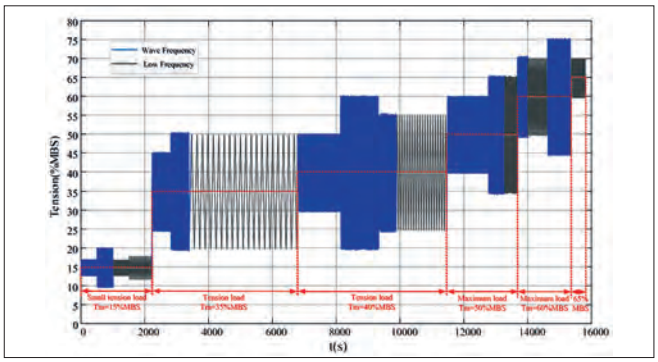

Fig. 8. Load curves for dynamic stiffness tests under working conditions

DYNAMIC STIFFNESS UNDER DIFFERENT TENSION AMPLITUDES

The pre-stretched rope was fixed on the tension-testing machine, and tests 8–10 were conducted to examine the influence of the tension amplitude (T_A) on the dynamic stiffness of the rope when the mean tension (T_m) was determined. The cyclic load acting on the rope was applied through the harmonic motion of the free end of the testing machine. Fig. 9 depicts the variation in force and strain with time. The figure indicates that the mean tension on the test rope was 40% MBS and the tension peak and tension valley were parallel, demonstrating that the test system could provide a long-term stable cyclic load of both the mean tension and the tension amplitude. The figure also shows that the strain increased with increasing tension amplitude; the strain is a maximum at T_A = 20% MBS.

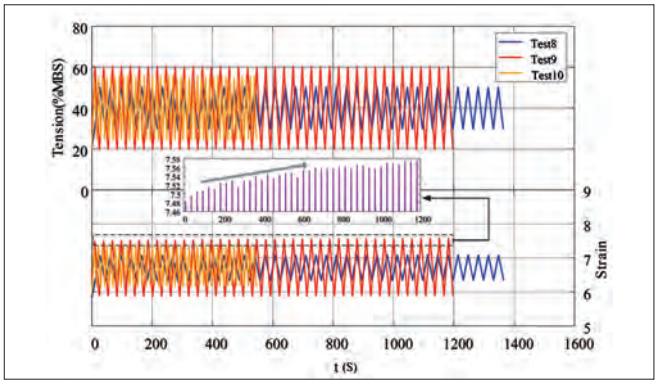

Fig. 9. Time curves of force and strain under different tension amplitudes

Fig. 10 shows the variation in rope tension and strain with time under different tension amplitudes (taking the results for the last five cycles, as an example). The test results show that the tension and strain change nonlinearly, and that a hysteresis loop forms owing to the nonlinear viscoelastic and viscoplastic behaviour. The area of the hysteresis loop represents the energy dissipation caused by the production and accumulation of the rope heat. In this test, a water-cooling system was used to cool the fibre rope, thus eliminating heat accumulation. The high degree of coincidence of the hysteresis loops in the last five cycles

indicates that the internal structure of the rope tends to be stable. The test also demonstrates that tension amplitude and strain are positively correlated and this result can be further extended to practical engineering. More specifically, the ability of a rope to resist dynamic deformation under high-amplitude loads is poor.

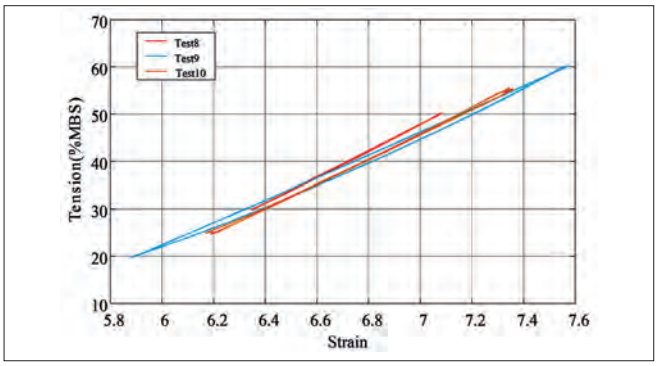

Fig. 10. Rope strains under different tension amplitudes in the last five cycles

Based on these tests, the evolution curve of the dynamic stiffness of polyester ropes with cyclic loads can be plotted using Eq. (2). Fig. 11 indicates that, even under tension amplitudes of 10%, 15%, and 20%, the effect of the tension amplitude on the dynamic stiffness is significant, and the tension amplitude and dynamic stiffness are negatively correlated. In particular, as the tension amplitude increases, the dynamic stiffness decreases. Therefore, the influence of the tension amplitude T_A cannot be ignored in the empirical formula for rope dynamic stiffness. At the same time, as the cycle load period increases, the fluctuation of the dynamic stiffness of the rope decreases, thus indicating a relatively stable internal structure of the cable rope. Thus, the dynamic stiffness of the rope, ultimately, tends to stabilise.

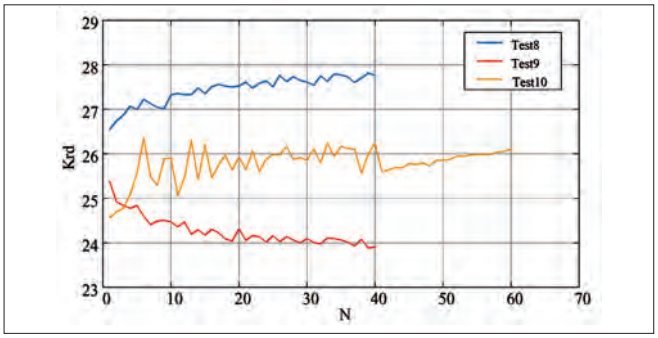

Fig. 11. Dynamic stiffness evolution under different tension amplitudes

DYNAMIC STIFFNESS UNDER DIFFERENT MEAN TENSIONS

Based on test conditions 7, 11, and 14, the influence of the mean tension (T_m) on the dynamic stiffness was examined. Fig. 12 shows the variations in the cyclic load and strain over time. When the load amplitude was 15% MBS, the strain ($\Delta L/L$) increased with increasing mean tension (T_m). Thus, the impact on the stability and deformation of the rope structure was greater under larger tension values. Combining the strain distribution of the rope under the last five cycles, as shown in Fig. 13, reveals that the residual strain accumulated in the initial stage of the test was considerable. With increasing time, the strain response to the cyclic load gradually reached a steady state and the hysteresis loops ultimately overlapped, indicating that the deformation of the rope tended to stabilise.

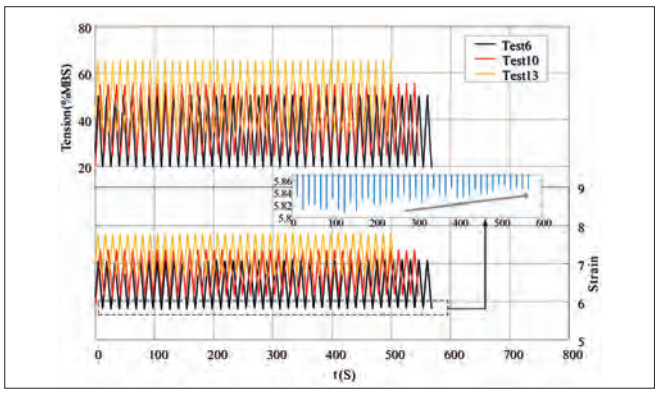

Fig. 12. Time curves of force and strain under different mean tensions

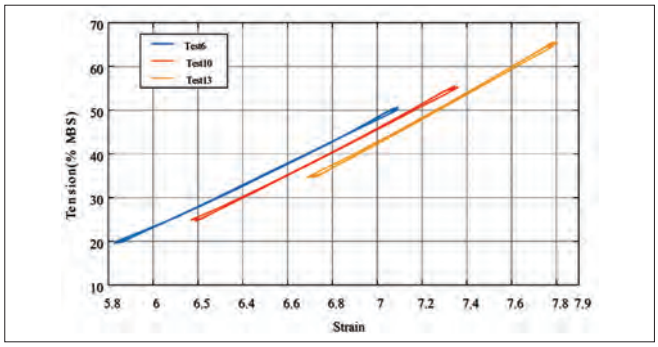

Fig. 13. Rope strains under different tension amplitudes in the last five cycles

Based on these experiments, the evolution curve of the dynamic stiffness of polyester ropes with periodic loads can be obtained by calculating and organising the test data using Eq. (2). Fig. 14 shows that the dynamic stiffness of the tested rope gradually increased with time and stabilised at $N = 40$; the dynamic stiffness of the rope was largest under $T_m = 50\%$ MBS, compared with the other two test conditions. In particular, the dynamic stiffness increased with an increase in the mean tension. The main reason for this was that the twisting changed the fibre structure inside the rope and was significant under a large load; the twisting angle between the structures decreased with an increase in the mean load. More specifically, the structure became more stable under high tension, owing to the smaller twisting angle between the fibres/strands. Thus, the rope had a greater ability to resist external deformation, thereby resulting in a larger dynamic stiffness.

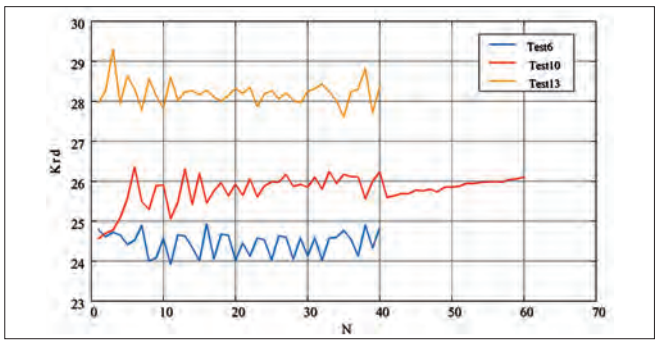

Fig. 14. Evolution of dynamic stiffness under different mean tensions

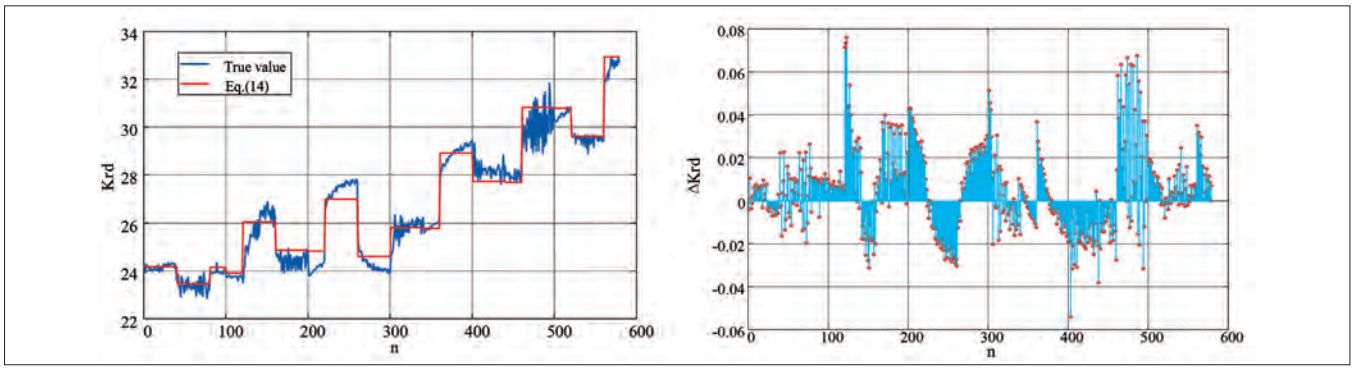

Fig. 15. Numerical analysis of rope dynamic stiffness: (a) dynamic stiffness value and (b) relative error

Based on the experimental data and the influence of the mean tension (T_m), tension amplitude (T_A), and load cycle (N), an empirical expression for the dynamic stiffness of polyester ropes was established, as shown in Eq. (12), where the parameters have the same meanings as previously mentioned.

$$K_{rd} = \alpha + \beta T_m + \gamma T_A + \delta \lg(N) \,. \tag{12}$$

Using the experimental data obtained under the 18 operating conditions designed in this test (Table 4), the relevant parameters in Eq. (17) were solved using the nonlinear fitting function in MATLAB, where α, β, γ, and δ were 21.87, 0.19, −0.24, and 0.04, respectively, as shown in Eq. (14).

$$K_{rd} = 21.87 + 0.19T_m - 0.24T_A - 0.04\lg(N) \,. \tag{14}$$

A comparison of the dynamic stiffness of the ropes is shown in Fig. 15, including the measured values $K_{rd,m}$ and the predicted values K_{rd} based on the empirical formulas. In Fig. 15(b), an error occurs between $N \approx 120$ and $N \approx 500$ rather than in the initial loading phase with the fastest growth rate. This is related to the relaxation and instability of the internal structure of the sample. When dynamic stiffness values are substituted into Eqs. 8) and (9), the calculated ME and MSE are 0.125 and 0.279, respectively. To a certain extent, this empirical formula can reflect the dynamic stiffness of polyester fibre ropes.

During the rope design phase, the use of predicted empirical formulas makes an advance estimation of stiffness possible, thereby reducing the need for extensive testing and lowering economic costs. To examine the flexibility of the different empirical equations for predicting the dynamic stiffness of polyester ropes, the measured dynamic stiffness (last cycle) was compared with the empirical equations under different conditions, as presented in Table 4. Clearly, the equation derived in this study provides the most-accurate calculations.

Fig. 16 indicates the existence of a significant error in Eqs. (4) 1 and (5); additionally, Eq. (4) 2 exhibits noticeable fluctuations. This indicates that the accuracy of the empirical equations used to predict the dynamic stiffness of the ropes is not entirely reliable. The determination of these empirical formulas may be influenced by such factors as the rope manufacturing processes, weaving structures, testing procedures, and equipment errors. Even with the same rope material, different weaving structures or testing procedures can lead to deviations in the predicted results of the empirical formulas. Therefore, further research is

Tab. 4. Comparison of measured and calculated values of dynamic stiffness of polyester ropes

Polyester	Measured K_{rd}	Eq. (4)		Eq. (5)	Eq. (14)
		1	2	1	1
Test 1	23.659	26.75	20.00	23.45	24.18
	Relative error (%)	13.06	15.47	0.88	2.20
Test 2	23.223	26.75	20.00	23.45	23.46
	Relative error (%)	15.19	13.88	0.98	1.02
Test 3	23.918	26.75	20.00	23.45	24.15
	Relative error (%)	11.84	16.38	1.96	0.97
Test 4	23.819	26.75	20.00	23.45	23.91
	Relative error (%)	12.31	16.03	1.55	0.38
Test 5	26.183	31.75	24.00	30.05	26.06
	Relative error (%)	21.26	8.34	14.77	0.47
Test 6	24.828	31.75	24.00	30.05	24.87
	Relative error (%)	27.88	3.34	21.03	0.17
Test 7	24.393	31.75	24.00	30.05	24.83
	Relative error (%)	30.16	1.61	23.19	1.79
Test 8	27.762	33.00	25.00	31.70	27.01
	Relative error (%)	18.87	9.95	14.18	2.71
Test 9	23.904	33.00	25.00	31.70	24.61
	Relative error (%)	38.05	4.58	32.61	2.95
Test 10	26.234	33.00	25.00	31.70	25.82
	Relative error (%)	25.79	4.70	20.84	1.58
Test 11	26.104	33.00	25.00	31.70	25.78
	Relative error (%)	26.42	4.23	21.44	1.24
Test 12	29.459	35.50	27.00	35.00	28.91
	Relative error (%)	20.50	8.35	18.81	1.86
Test 13	28.354	35.50	27.00	35.00	27.72
	Relative error (%)	25.20	4.77	23.44	2.24
Test 14	28.466	35.50	27.00	35.00	27.68
	Relative error (%)	24.71	5.15	22.95	2.76
Test 15	30.337	38.00	29.00	38.30	30.82
	Relative error (%)	25.26	4.41	26.25	1.59
Test 16	30.836	38.00	29.00	38.30	30.78
	Relative error (%)	23.23	5.95	24.21	0.18
Test 17	29.418	38.00	29.00	38.30	29.61
	Relative error (%)	29.17	1.42	30.19	0.65
Test 18	32.714	39.25	30.00	39.95	32.93
	Relative error (%)	19.98	8.30	22.12	0.66

needed to improve the universality of these empirical formulas for predicting rope dynamic stiffness.

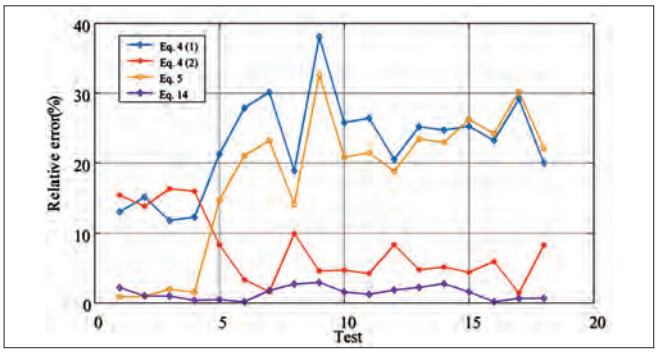

Fig. 16. Comparison of results from empirical formulas for dynamic stiffness of ropes

CONCLUSION

To study the tensile properties and stiffness characteristics of polyester fibre ropes, several tensile tests were conducted. The mechanical characteristics of the ropes were explored under static loads during three stages: preloading, initial installation, and aging. The experimental results demonstrated a positive correlation between the elongation rate and the tensile strength of the ropes. A reversible elongation rate of approximately 0.23% was observed during the preloading stage under small loads. By contrast, the reversible elongation rates during the initial installation and aging stages under large loads were similar (approximately 0.45%). This indicates that the axial force disrupts the internal structure of the ropes; however, once they are sufficiently worn, the elongation rate and reversible elongation rate tend to stabilise at a fixed value.

To facilitate the prediction of the static stiffness during the design phase, an empirical formula for the static stiffness of polyester ropes was established based on the creep coefficient. We found that the static stiffness of the rope is linearly correlated with the duration of the load. Furthermore, the aged ropes had a higher static stiffness than the initially installed ropes. This is mainly attributed to the fact that the ropes that had been used underwent sufficient stretching, resulting in a smaller residual strain and a more stable structure, thus leading to increased stiffness. Comparing the creep coefficients under different loads revealed that the coefficient increases as the load increases.

The cyclic load test considered the effects of different mean loads and load amplitudes on the dynamic stiffness of the rope. The dynamic stiffness increased with an increase in the mean load and decreased with an increase in the load amplitude. An empirical formula for the dynamic stiffness was established and multiple empirical formulas were compared with experimental measurements. Overall, all of the empirical formulas significantly underestimated the dynamic stiffness. The determination of empirical formulas is influenced greatly by such factors as the rope manufacturing process, braiding structure, testing procedure, and equipment errors.

REFERENCES

1. D. Vecchio and C.J. Moraes, 'Light weight materials for deep water moorings', University of Reading, 1992.
2. R.S. Kota, W. Greiner, and R.B.D'Souza, 'Comparative assessment of steel and polyester moorings in ultradeep water for spar- and semi-based production platforms', Proceedings of the Offshore Technology Conference. 1999, https://doi.org/10.4043/10909-MS.
3. G.P. Foster, 'Advantages of fibre rope over wire rope', Journal of Industrial Textiles. 2002, doi: 10.1106/152808302031656.
4. American Bureau of Shipping, 'Guidance notes on the application of fibre rope for offshore mooring'. 2011.
5. J.F. Beltran and E.B. Williamson, 'Degradation of rope properties under increasing monotonic load'. Ocean Engineering. 2005, https://doi.org/10.1016/j.oceaneng.2004.10.004.
6. J.F. Beltran and E.B. Williamson, 'Investigation of the damage-dependent response of mooring ropes', Journal of Engineering Mechanics. 2009, https://doi.org/10.1061/(ASCE)0733-9399(2009)135:11(1237).
7. J.F. Beltran and E.B. Williamson, 'Numerical simulation of damage localization in polyester mooring ropes'. Journal of Engineering Mechanics. 2010, https://doi.org/10.1061/(ASCE)EM.1943-7889.0000129.
8. J.G. Williams, A. Miyase, D. Li, and S.S. Wang, 'Small-scale testing of damaged synthetic fibre mooring ropes'. Proceedings of the Offshore Technology Conference. 2002, https://doi.org/10.4043/14308-MS.
9. E.G. Lanquetin, R.R. Ayers, S.J. Banfiel, N. O'Hear, C.E. Smith, and T. Laurendine, 'The residual strength of damaged polyester rope'. Proceedings of the Offshore Technology Conference. 2006, https://doi.org/10.4043/18150-MS.
10. Y. Lian, B. Zhang, J. Zheng, H. Liu, G. Ma, S.C. Yim, and Y. Zhao, 'An upper and lower bound method for evaluating residual strengths of polyester mooring ropes with artificial damage'. Ocean Engineering. 2022, https://doi.org/10.1016/j.oceaneng.2022.112243.
11. P. Davies, Y. Reaud, L. Dussud, and P. Woerther, 'Mechanical behaviour of HMPE and aramid fibre ropes for deep sea handling operations'. Ocean Engineering. 2011, https://doi.org/10.1016/j.oceaneng.2011.10.010.
12. G. Li, W. Li, S. Lin, H. Li, Y. Ge, and Y. Sun, 'Dynamic stiffness of braided HMPE ropes under long-term cyclic loads: A full-scale experimental investigation'. Ocean Engineering. 2021, https://doi.org/10.1016/j.oceaneng.2021.109076.

13. C. Bain, P. Davies, G. Bles, Y. Marco, and J. Barnet, 'Influence of bedding-in on the tensile performance of HMPE fibre ropes'. Ocean Engineering. 2020, https://doi.org/10.1016/j.oceaneng.2020.107144.

14. P. Davies, M. François, F. Grosjean, P. Baron, K. Salomon, and D. Trassoudaine, 'Synthetic mooring lines for depths to 3000 meters'. Proceedings of the Offshore Technology Conference. 2002, https://doi.org/10.4043/14246-MS.

15. H. Liu, W. Huang, Y. Lian, and L. Li, 'An experimental investigation on nonlinear behaviours of synthetic fibre ropes for deepwater moorings under cyclic loading'. Applied Ocean Research. 2014, https://doi.org/10.1016/j.apor.2013.12.003.

16. Y. Lian, H. Liu, L. Li, and Y. Zhang, 'An experimental investigation on the bedding-in behaviour of synthetic fibre ropes'. Ocean Engineering. 2018, https://doi.org/10.1016/j.oceaneng.2018.04.071.

17. S. Xu, S. Wang, H. Liu, Y. Zhang, L. Li, and C.G. Soares, 'Experimental evaluation of the dynamic stiffness of synthetic fibre mooring ropes'. Applied Ocean Research. 2021, https://doi.org/10.1016/j.apor.2021.102709.

18. S. Xu and C. Guedes Soares, 'Dynamics of an ultra-deepwater mooring line with embedded chain segment'. Marine Structures. 2020, https://doi.org/10.1016/j.marstruc.2020.102747.

19. S.D. Weller, L. Johanning, P. Davies, and S.J. Banfield, 'Synthetic mooring ropes for marine renewable energy applications'. Renewable Energy. 2015, https://doi.org/10.1016/j.renene.2015.03.058.

20. W. Huang, H. Liu, Y. Lian, and L. Li, 'Modeling nonlinear creep and recovery behaviours of synthetic fibre ropes for deepwater moorings'. Applied Ocean Research. 2013, https://doi.org/10.1016/j.apor.2012.10.004.

21. L. Maoben, L. Yanxi, L. Hangyu, L. Ji, '3000 tons and below rope tension reciprocating tester'. Patent CN108548738A.

22. M. Francois and P. Davies, 'Characterization of polyester mooring lines'. Proceedings of the ASME International Conference on Offshore Mechanics & Arctic Engineering. 2008.

23. C. Wibner, T. Versavel, and I. Masetti, 'Specifying and testing polyester mooring rope for the Barracuda and Caratinga FPSO deepwater mooring systems'. Proceedings of the Offshore Technology Conference. 2003, OTC-15139-MS.

24. H. Liu, Y. Lian, L. Li, Y. Zhang, 'Experimental investigation on dynamic stiffness of damaged synthetic fibre ropes for deepwater moorings. Journal of Offshore Mechanics and Arctic Engineering. 2015.